Identification of Nitrogen Dopants in Single-Walled Carbon Nanotubes by Scanning Tunneling Microscopy

Yann Tison,[*,†,‡] Hong Lin,[†,‡] Jérôme Lagoute,[*,†] Vincent Repain,[†] Cyril Chacon,[†] Yann Girard,[†] Sylvie Rousset,[†] Luc Henrard,[¶] Bing Zheng,[¶] Toma Susi,[§] Esko I. Kauppinen,[§] François Ducastelle,[‡] and Annick Loiseau[‡]

[†]Laboratoire Matériaux et Phénomènes Quantiques, UMR7162, Université Paris Diderot-Paris 7, Sorbonne Paris Cité, CNRS, UMR 7162 case courrier 7021, 75205 Paris Cedex 13, France, [‡]Laboratoire d'Etude des Microstructures, ONERA-CNRS, BP 72, 92322 Châtillon Cedex, France, [¶]Department of Physics, University of Namur, 61 rue de Bruxelles, 5000 Namur, Belgium, and [§]Nanomaterials Group, Department of Applied Physics, Aalto University School of Science, P.O. Box 15100, 00076 Aalto, Finland

ABSTRACT Using scanning tunnelling microscopy and spectroscopy, we investigated the atomic and electronic structure of nitrogen-doped single walled carbon nanotubes synthesized by chemical vapor deposition. The insertion of nitrogen in the carbon lattice induces several types of point defects involving different atomic configurations. Spectroscopic measurements on semiconducting nanotubes reveal that these local structures can induce either extended shallow levels or more localized deep levels. In a metallic tube, a single doping site associated with a donor state was observed in the gap at an energy close to that of the first van Hove singularity. Density functional theory calculations reveal that this feature corresponds to a substitutional nitrogen atom in the carbon network.

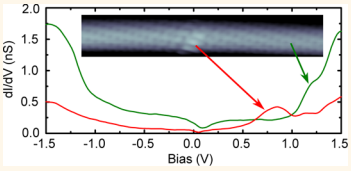

KEYWORDS: carbon nanotubes · nitrogen-doping · electronic structures · scanning tunneling microscopy and spectroscopy · density functional theory

The discovery of carbon nanotubes (CNTs)[1] raised considerable interest in both the experimental and theoretical research communities,[2,3] and their unique properties gave birth to numerous potential applications in various fields including energy storage, composite materials, and nanoelectronics.[3] The electronic properties of single-walled carbon nanotubes (SWNTs)—in particular their metallic or semiconducting character—are controlled by their chirality, described by the coordinates of the chiral vector (*n*,*m*). Despite intense research, synthesizing nanotubes with well-defined properties remains a challenging task. One strategy for tailoring their physical or chemical properties is to dope them with foreign atoms incorporated in the carbon lattice.[4] Thanks to its appropriate atomic radius, nitrogen can easily fit into the carbon honeycomb lattice, and its additional electron compared to carbon suggests a donor character.[4,5] Doping CNTs with nitrogen is a promising way for tailoring their properties for applications in field emission,[6] nanoelectronics,[7] gas sensing,[8] or catalysis.[9]

While many experimental efforts have focused on N-doped multiwalled CNTs,[4,5] it should be stressed that nitrogen-doped SWNTs have been significantly less studied. Only few studies have reported the synthesis of N-doped SWNTs using arc discharge,[10] chemical vapor deposition,[11,12] or laser vaporization techniques.[13,14] For both MWNTs[15] and SWNTs,[12−14,16] X-ray photoelectron spectroscopy (XPS) and electron energy loss spectroscopy (EELS) measurements have provided evidence for the presence of at least two atomic bonding configurations of the nitrogen dopant atoms, commonly referred to as graphitic and pyridinic. The first one designates a 3-fold coordinated nitrogen atom simply substituting a carbon atom in the lattice, and the latter a 2-fold coordinated nitrogen with one p electron contributing to the π system. The influence of these two local environments for nitrogen was recently investigated using density functional theory (DFT) calculations,[17] which indicated that graphitic nitrogen atoms induce an n-type doping of the carbon host, whereas pyridinic ones induce p-type doping, as proposed earlier.[18] A good understanding of the type of doping that can be achieved in SWNTs—especially in the semiconducting tubes—is crucial for their

* Address correspondence to yann.tison@univ-paris-diderot.fr, jerome.lagoute@univ-paris-diderot.fr.

Received for review May 23, 2013 and accepted July 5, 2013.

Published online July 05, 2013
10.1021/nn4026146

potential applications in nanoelectronics. This requires an in-depth knowledge of the bonding of the nitrogen atoms incorporated in the carbon lattice.

Scanning tunneling microscopy (STM) and spectroscopy (STS) are well-suited for investigating the structure and properties of carbon nanotubes.[19,20] Theoretical investigations[17] also included simulations of scanning tunneling microscopy images, suggesting that the changes of the electronic structure of SWNTs due to nitrogen doping could be detected with this technique. STM measurements on nitrogen-doped multiwalled carbon nanotubes showed the presence of lattice defects in the STM images, which were attributed to clusters of nitrogen atoms in a pyridinic-like environment.[21] In more recent STM experiments performed on nitrogen-doped SWNTs prepared by a laser ablation method,[13,22] the doping sites appeared as local protusions in the STM images, surrounded by interference patterns with a periodicity of 0.44 nm. Although nitrogen atoms in the substitutional configuration have been recently identified in N-doped graphene,[23−26] their direct detection in carbon nanotubes has remained elusive until now.

In this study, we report on the results of a low-temperature STM and STS investigation of N-doped SWNTs, with close support from theoretical modeling. For the first time, we identify a substitutional (graphitic) nitrogen atom in a carbon nanotube. As theoretically predicted, this configuration gives a donor level close to the first van Hove singularity of its metallic nanotube host. We also evidence the presence of other types of point defects related to nitrogen doping. These defects can be quite complex and they exhibit either deep or shallow levels in the density of states. Finally, our data reveal the presence of long-range perturbations of the nanotube wave functions due to scattering by the point defects.

RESULTS AND DISCUSSION

In Figure 1, typical STM images of nitrogen-doped single-walled carbon nanotubes deposited on a polycrystalline gold substrate are shown. The large scale image (Figure 1a) displays a bundle of N-doped SWNTs. In the bottom left corner of Figure 1a, one can also observe a series of steps belonging to the Au substrate. The height of these steps (0.25 nm) is in good agreement with the distance between two (111) atomic planes in gold. The top right corner of the image, on the contrary, exhibits grains that we attribute to catalyst nanoparticles or amorphous carbon deposited on the substrate during sample preparation. On the surface of the nanotube bundle, several point defects can be observed as small protusions or as distortions of the atomic lattice; these are more visible on the derivative image shown in Figure 1b. It is important to mention here that such defects have never been observed for nanotubes synthesized with the same method in the absence of NH_3 in the feed gas.[27,28] Furthermore, XPS and EELS measurements have demonstrated the presence of nitrogen with an unhomogenous distribution along the tubes in this batch of N-doped SWNTs.[29] Therefore, we are confident that the point defects observed in STM can be assigned to doping sites with one or several nitrogen atoms inserted into the carbon honeycomb lattice. In Figure 1c,d, we focus our attention on one of the point defects, located in the top left corner of Figure 1a. The topographic image and its derivative both exhibit the atomic lattice corresponding to the carbon honeycomb network, where the doping site is observed as a 0.7 nm wide protusion, together with a local lattice distortion that extends over the tube circumference. Another example displayed in Figure 1e,f shows a nanotube with two doping sites separated by approximately 10 nm. Both defects appear as large protusions (1.7 nm wide) and, similarly to the previous example, their influence is spread over the whole circumference of the tube.

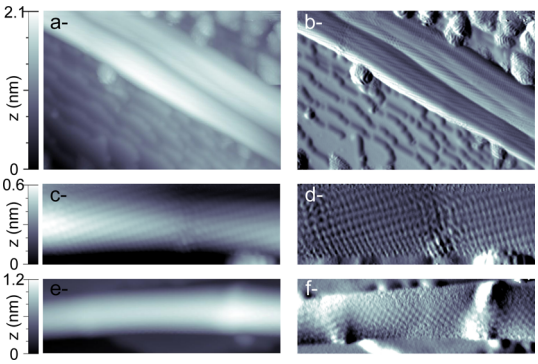

Figure 1. (a) Topographic image (30 × 20 nm^2) of a bundle of N-doped single-walled carbon nanotubes deposited on a Au/glass substrate, sample voltage +1.50 V, tunneling current 50 pA; (b) derivative image of panel a; (c) smaller scale topographic image (10 × 4 nm^2) of a single point defect of a N-doped nanotube belonging to the bundle shown in panels a and b, sample voltage +1.50 V, tunneling current 200 pA; (d) derivative image of panel c; (e) topographic image (16 × 5 nm^2) of another N-doped single-walled carbon nanotube presenting two doping sites separated by *ca.* 10 nm, sample voltage +0.70 V, tunneling current 100 pA; (f) Derivative image of panel e.

For a more comprehensive description of the doping sites in N-doped SWNTs, an STS study of several point defects was undertaken. For most of the cases we observed, the topographic and spectroscopic signatures are quite complex. However, we succeeded to comprehensively characterize a simple and well-defined point defect in one doped nanotube, whose properties are depicted in Figure 2.

The topographic image (12 × 3 nm^2) in Figure 2a, recorded with a sample bias of +1.0 V, displays two single-walled carbon nanotubes on the gold substrate. Nanotube A (at the top of the image) does not present any defect in the scanned area, whereas nanotube B (at the bottom) exhibits a localized doping site. The diameter and chiral angle of Nanotube A are

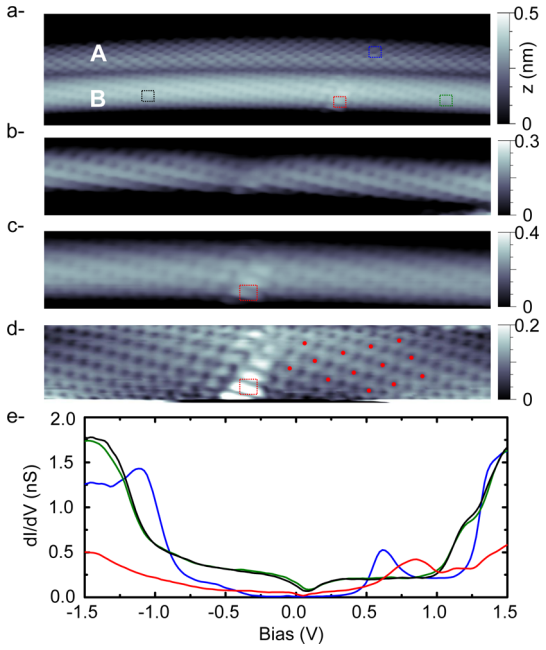

Figure 2. (a) (12 × 3 nm^2) constant current image of two SWNTs labeled A and B, one of which (B) presents a defect (sample voltage V_s = +1.00 V, tunneling current I_t = 200 pA). (b) (7 × 1.2 nm^2) constant current image of the defect observed in image a at V_s = −1.00 V, (c) (7 × 1.2 nm^2) constant current image of the defect observed in image a at V_s = +1.00 V with a tunneling current of 200 pA, (d) STM image shown in panel c corrected by a line-by-line flattening; the red dots indicate the periodicity of a superstructure donut pattern; (e) tunneling spectra acquired on the two tubes shown in image a. The blue curve was measured on the tube A; the black and green curves were measured on the pristine part of tube B. The red curve was measured on tube B at the defect's location. The colored boxes in image a represent the points where the spectra were recorded (the red box for the STS measurement on the N-induced defect is repeated in images c and d).

1.1 nm and 13°, respectively, associated with a (12,4) semiconducting SWNT. For nanotube B, a diameter of 1.1 nm and a chiral angle of 17° are measured, which correspond to a (11,5) SWNT. The magnified images (7 × 1.2 nm^2) in Figure 2b,c reveal the bias dependence of the topographic signature of this defect. It appears as a depletion at negative bias (−1 V) and as a protusion at positive bias (+1 V). This protrusion is 0.6 nm wide in the direction of the tube main axis and is spread over the visible part of the tube circumference. In Figure 2d, we show the image recorded at +1 V (Figure 2c) after a flattening procedure. This allows a better view of the doping site and a series of four parallel bright segments separated by 0.24 nm, this structure for the doping site will be analyzed later in the paper with the support of theoretical calculations. On this flattened image, a superstructure donut pattern is also observed, as indicated by the red dots in Figure 2d, this type of pattern is predicted in the vicinity of point defects for nanotubes[17] and graphene nanoribbons[30] and this point will be discussed later in the paper.

In addition, we probed the electronic structure of these two tubes by measuring the local tunneling spectra shown in Figure 2e. First, a spectrum representative of nanotube A (blue line) exhibits a zero density of states at the Fermi level, with the first van Hove singularities typical of a semiconducting nanotube observed at approximately −0.4 V and +0.5 V. The resulting bandgap of 0.9 V corresponds to the expected range for a nanotube with a diameter close to 1.1 nm when the screening by the Au substrate is taken into account.[27] On this spectrum, the second van Hove singularities are observed at −0.9 V and +1.3 V. For nanotube B, spectra acquired on the pristine parts of the tube (black and green curves), more than 4 nm from the doping site on either side, show the first van Hove singularities at −1.2 V and +1.1 V and a pseudogap at the Fermi level, characteristic of a metallic chiral nanotube.[31] The 2.3 V separation between the first two van Hove singularities corresponds to the tabulated value for a metallic SWCNT with a 1.1 nm diameter.[32] The spectrum recorded on top of the defect (red curve) shows an additional state with a broad contribution centered at 0.8 V and less prominent van Hove singularities. This experimental signature was predicted in a recent DFT study for a nitrogen atom substituting a carbon atom in the honeycomb lattice.[17] Specifically, the calculations showed that the donor state of a nitrogen substitution appears 0.2 eV below the first van Hove singularity in the conduction band of a (10,10) metallic tube; despite the fact that this behavior is not directly comparable to the experimental data in Figure 2 since the chirality and diameter affect the energies of the van Hove singularity. This interpretation is strengthened by recent studies performed on N-doped graphene[25] and on N-doped graphite,[33] where the spectra corresponding to substitutional nitrogen atoms display additional contributions in the conduction band (0.5 V above E_F). Therefore, the signature observed in Figure 2 is attributed to a substitutional nitrogen atom in a single-walled carbon nanotube.

To verify this assignment for the results presented in Figure 2 and to extend the theoretical work reported by Zheng and co-workers,[17] DFT calculations were performed on a (11,5) carbon nanotube with a single subtitutional N atom. In Figure 3, we present two theoretical STM images computed within the framework of the Tersoff−Hamann model[34,35] for sample biases of −1 V and +1 V, together with the DOS for the N-doped (11,5) carbon nanotube. As a reference, the total DOS computed for a pristine (11,5) nanotube is also presented.

For a bias of −1 V (Figure 3a), the calculated image exhibits a dip around the nitrogen dopant atom, characteristic of a lower local density of states (LDOS) compared to the carbon atoms. On the contrary, the theoretical image calculated at +1 V (Figure 3b) shows an increased LDOS and therefore apparent protrusions located on the nearest carbon atoms, belonging to the

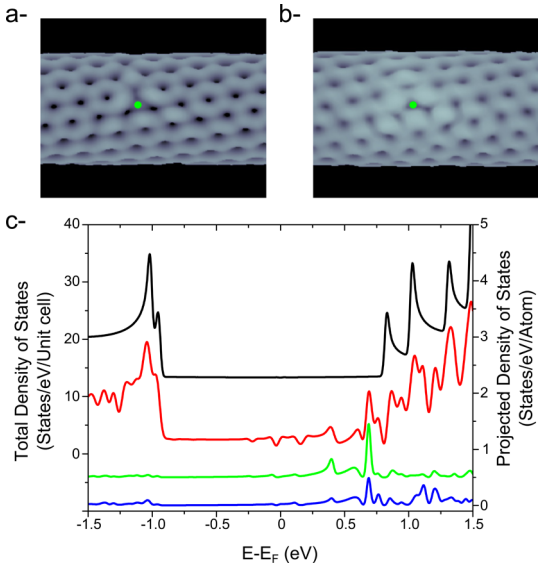

Figure 3. (a,b) Theoretical STM images (20.13 Å × 16.18 Å of a N-doped single-walled (11,5) chiral carbon nanotube at sample bias of (a) −1.0 V and (b) +1.0 V, the location of the N atom is indicated by green dots. (c) Density of states for a pristine (11,5) nanotube (black), a N-doped (11,5) carbon nanotube (red), and the projected density of states (PDOS) on the nitrogen atom (green) and on a first neighbor carbon atom (blue) in the N-doped nanotube. The total DOS are shown in units of states/eV/unit cell (left-hand scale) and the projected DOS in units of states/eV/atom (right-hand scale). For better clarity, Y-offsets of 11 states/eV/unit cell and 0.5 states/eV/atom have been applied to the black curve and the green curve, respectively. The total DOS and the projectected DOS for the N-doped (11,5) carbon nanotube have been shifted by 0.15 eV for an easier comparison with the pristine tube.

sublattice of the first neighbors of the nitrogen atom. This feature, also observed in graphene with nitrogen substitutions,[23−25] corresponds to an apparent width of approximately 1 nm in the modeled image. The observed small dip at negative bias and a protrusion at positive bias are in good agreement with the trend observed in the zoomed images presented on Figure 2b,c. It is also to be noted that the N atom appears as a very localized hole on the theoretical image at +1 V. This had been previously assigned to a stronger localization of the DOS around the nucleus of the N atom with respect to carbon atoms, as well as to a charge transfer to the neighboring carbon atoms.[17]

In contrast with experimental observations of substitutional nitrogen atoms in graphene,[23,25] and with calculated images in Figure 3, the protrusions in our STM images in Figure 2 do not display a clear triangular pattern. This is likely due to the location of the N atom along the circumference of the tube with respect to the STM tip. The overall shape of the protrusion suggests that it is not facing directly the STM tip, but is is rather located on the side of the tube, or even on its underside. Furthermore, in the image recorded at +1 V, intensity maxima related to the protrusions build a fringe pattern (i.e., the bright parallel segments separated by 0.24 nm in Figure 2d) with a periodicity corresponding to the spacing between atoms belonging to a given sublattice. This spacing is also that of the protrusions visible in the calculated STM image at +1.0 V along the edges of the triangular pattern. As shown by recent calculations performed for N-doped graphene,[36] this pattern arises from the redistribution of the density of states from the N atom to its first and third neighboring carbon atoms (and to C atoms on the same sublattice). This suggests that in the experimental situation, the N atom is located in such a way that only one edge of the triangle is facing the STM tip, leading to the apparent fringe contrast. A triangular shape for a point defect located on the top side of a nanotube could very rarely be observed and one example is shown in Supporting Information (Figure S1). However, we could not determine its chemical nature, due to the lack of spectroscopic data. We note here that the simulated triangular pattern (with a central hole) is not systematically observed experimentally for substitutional N atoms in sp^2 nanomaterials, as recently illustrated by STM investigations of N-doped graphene.[25] This discrepancy between experiments and theoretical modeling is a consequence of the variation of the LDOS far from the atoms. Indeed, the STM images depend on the LDOS at the top position, typically 5 Å to 10 Å from the sample surface where numerical analysis with DFT is restricted to distances smaller than 5 Å. More information on that point is given as Supporting Information (Figure S2).

The spectroscopic signature of the doping site (Figure 2e) is modeled by the density of states (Figure 3c) calculated for a N-doped (11,5) carbon nanotube (red), whereas the calculated DOS of a pristine (11,5) carbon nanotube (black) is used to simulate the STS spectra recorded away from the defect. Both curves exhibit the first van Hove singularities at −1.0 eV and +0.8 eV, in reasonable agreement with the experimental data. The DOS for the N-doped nanotube also displays an additional contribution centered around +0.6 eV, which matches well with the peak observed experimentally at the defect location. The projected densities of states for the nitrogen atom and for the nearest carbon atoms are plotted in green and blue, respectively. They show that this donor state at 0.6 eV is localized on these two types of atoms. This is also in agreement with the charge transfer from the N atom to its first neighbors discussed previously. The small difference between the calculated and measured energy separating the first van Hove singularities and the localized states can be understood by the inherent limitations of DFT−LDA (see Barone *et al.*[37] for nanotubes) and, more precisely, by the fact that the electron−electron correlation could be different for delocalized carbon states and N-induced localized states. In addition, the tube−substrate interaction that can lead to a renormalization of the electronic spectrum is not taken into account in the simulations (although this effect is small in the case of metallic nanotubes).[27]

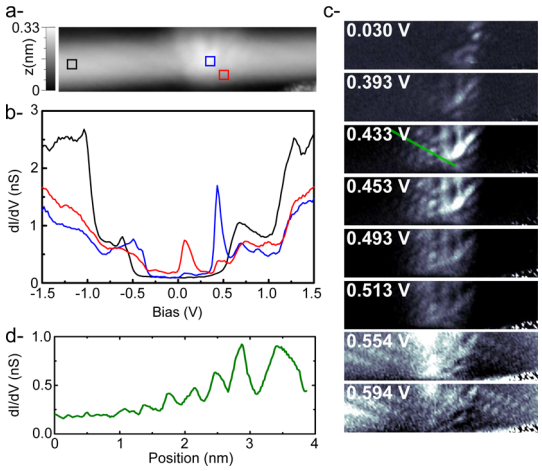

Figure 4. (a) Constant current image of a SWNT presenting a defect induced by nitrogen doping (8 × 2 nm^2, sample voltage V_s = +1.00 V, tunneling current I_t = 500 pA). (b) Tunneling spectra recorded 3 nm away from the defect (black), at the center of the defect (blue), and on the right-hand side of the defect (red) (V_s = +1.00 V, I_t = 500 pA). The locations corresponding to the spectra are indicated by the colored boxes in panel b. (c) Differential conductance maps recorded at various bias voltages during a CITS (current imaging tunneling spectroscopy) experiment on the image shown in panel a; the imaging conditions were V_s = +1.00 V and I_t = 500 pA. (d) A line profile recorded along the green line on the differential conductance map at +0.433 V in panel b.

Moreover, the structure of most of the doping sites we observed was rather complex, and an example is presented in Figure 4. In the topographic image (Figure 4a), the defect appears as a 0.1 nm high protrusion, which extends over 2.5 nm along the nanotube axis and over the observable part of its circumference. To further investigate the electronic structure of this defect, spectroscopic measurements are displayed in Figure 4b and Figure 4c. The spectra recorded on the pristine part of the nanotube (black curve in Figure 4b) exhibit a nearly zero density of states around the Fermi level and two pairs of contributions at −0.6 V and +0.6 V for the first van Hove singularities and −1.0 V and +1.1 V for the second ones, typical of a semiconducting nanotube. Again, the bandgap of 1.2 eV lies within the expected range considering the screening by the Au substrate.[27] In the defective area, the tunneling spectra reveal two additional features at +0.07 V and +0.43 V. The relative intensities of these peaks vary depending on the location where the spectrum is recorded. The distance of 0.7 nm between the measured maxima of the LDOS is much larger than the C−C interatomic distance. The doping site is therefore most likely a combination of two different defects, one leading to a deep level (*i.e.*, in the center of the bandgap), the other to a shallow level (*i.e.*, close to the conduction band). Considering the data presented in Figure 2 and Figure 3 and the discussed theoretical analysis,[17] the shallow level at +0.43 V can reasonably be assigned to a N atom in substitution.

Regarding the state associated with the peak near the Fermi level, two structures can be considered. Recent studies involving STM/STS[38] and theoretical calculations[38−40] show that vacancy defects appear as hillock structures in the images and that a single peak at the Fermi level is observed in the STS spectra. This signature makes single or double vacancies good candidates for explaining the presence of a state in the midgap region. The second possible structure involves three nitrogen atoms surrounding a vacancy (pyridinic configuration), for which the DOS also shows a single peak in the vicinity of the Fermi level for a nonchiral semiconducting tube of similar diameter,[17] as shown by the DOS calculated for a pyridinic site (see Supporting Information). Since pyridinic nitrogen atoms were detected by EELS and XPS in these samples, this configuration without any dangling bonds seems a more likely explanation. In Figure 4c, we show a series of differential conductance maps as a function of the bias voltage. These maps reveal variations in the spatial distribution of the LDOS with respect to energy. The two defects are too close (less than 1 nm) to obtain individual images of the induced electron density redistribution. The state corresponding to the peak close to the deep level (+0.07 V) is localized around the circumference of the tube (it is spread over less than 1 nm along the direction of the nanotube axis). On the contrary, the shallow state at +0.43 V has a larger spatial extension of over 3 nm along the tube axis.

An additional key feature emerging from this series of conductance maps is a superstructure with a periodicity of 0.44 nm, as indicated by the line profile in the inset of Figure 4d. This pattern corresponds to a redistribution of the DOS over the carbon atoms of the sublattice not containing the N atom, with a $\sqrt{3}a \times \sqrt{3}a$ periodicity (a being the lattice parameter of the graphene sheet). The spatial extension of this modulation progressively increases when the bias energy approaches that of the van Hove singularity. The conductance maps recorded at 0.554 and 0.594 V exhibit a long-range modulation of the DOS, also with a $\sqrt{3}a \times \sqrt{3}a$ periodicity. Since the wave functions close to the Dirac K points indeed have this periodicity, the modulation is typical of the electronic perturbation induced by local defects in graphitic structures, carbon nanotubes in particular.[39,41−45] More precisely, in a simple tight-binding model, the amplitudes at sites $\vec{n}$ of the Bloch states of energy $\propto |\vec{q}|$ are proportional to $\exp i(\pm\vec{K} \pm\vec{q})\cdot\vec{n}$. In such a one-dimensional system, these states can be viewed as a set of two forward and two backward propagating states. For pristine systems, the stationary states have the full symmetry of the considered nanotubes. In the presence of localized defects, however, interference between forward and backward waves are produced, and since $|\vec{q}| \ll |\vec{K}|$, the corresponding modulation is driven by $\vec{K}$ and produces a $\sqrt{3}a \times \sqrt{3}a$ periodicity. For a given energy, the

range of the perturbation is in principle infinite, which is why it cannot usually be obtained by first principles calculations such as those shown in Figure 3 which are limited to small unit cell sizes.

In practice, the presence of other defects and the energy window used in the CITS (current imaging tunneling spectroscopy) spectra (10 mV) introduce damping effects. A full theoretical analysis based on a Green function formalism shows that the effect should be enhanced close to van Hove singularities as observed here.[39] Additionally, the precise motif of the $\sqrt{3}a \times \sqrt{3}a$ modulation should depend on the chiral angle, which is why various contrast modulations have been observed in the vicinity of defects.[41,43,44] Such a modulation is also found to occur for the defect shown in Figure 2d, the superstructure donut pattern visible in the magnified image being enhanced thanks to recording conditions at a voltage close to a van Hove singularity. In the image, the donut shapes can be seen around the red markers in Figure 2d. It is to be noted that a similar donut pattern has been evidenced on the theoretical images calculated by Zheng and coworkers[17] for the back side of a (10,10) nanotube, with respect to the nitrogen atom. This periodicity is the same $\sqrt{3}a \times \sqrt{3}a$ periodicity observed in Figure 4c.

The results reported here bring new experimental insights on the nature and properties of the doping sites in N-doped carbon nanotubes, down to the subnanometer scale. This local picture is complementary of the mesoscopic or macroscopic characterization provided by other techniques. From a structural point of view, XPS[16] and EELS[13,14] measurements have provided evidence for the presence of pyridinic and substitutional nitrogen atoms, which is in agreement with the STM and STS signatures reported here. Moreover, the random distribution of N-induced defects illustrated by Figure 1 is consistent with the unhomogenous nitrogen concentration along the tubes as shown by a recent EELS study. In terms of transport properties, DFT calculations performed for nitrogen doped nanotubes[46] predict a lower quantum conductance at the energy of the donor state (compared to a pristine tube), together with a decrease of the electrons' mean free path as a function of dopant's concentration. From the experimental point of view, four-point sheet resistance measurements of thin films of the N-doped nanotube samples studied here showed an increase of resistance as the doping level goes up.[29] This behavior may partially be explained by the decrease of conductance predicted from DFT[46] at the energy of the donor state, but also by the lower mean free path in doped nanotubes, which we associate to the N-induced defects acting as scattering centers. Independently, the four-point conductivity measurements performed by Villalpando-Paez and co-workers[11] provided evidence for the presence of both deep and shallow levels in N-doped carbon nanotubes prepared by pyrolysis of a ferrocene/ethanol/benzylamine solution. These macroscopic measurements are in strong agreement with the nanometer-scale data presented in Figure 4, which exhibits two peaks at the Fermi level and close to the van Hove singularity. Finally, it is to be noted that the current−voltage characteristics measured for isolated nitrogen-doped nanotubes have demonstrated that n-type doping is achievable, provided that the concentration of substitutional nitrogen atom, like the case displayed in Figure 2, is sufficient.[7,47]

CONCLUSIONS

To summarize, we performed a low temperature STM/STS investigation of nitrogen-doped single-walled carbon nanotubes. The topography of the point defects associated with the presence of nitrogen dopants appears as hillocks. Furthermore, local spectroscopy reveals that the doping sites lead to the formation of electronic states at energies lying between the two first van Hove singularities. A few nanometers from these point defects, the LDOS features of the pristine nanotubes are recovered. The atomic configuration of the doping sites can vary from substitutional N atoms to more complex cases. For a single substitutional N atom, the spectroscopic data agrees closely with our first principles calculations, showing a broad donor state slightly below the energy of the van Hove singularity. A combined point defect, on the other hand, exhibits both deep and shallow levels, respectively localized (spread over less than 1 nm) or extended (spread over 3 nm) around the dopant in a semiconducting tube. The deep level probably involves pyridinic nitrogen atoms that were previously detected by EELS and XPS. Finally, we observed a long-range modulation of the nanotubes' wave functions corresponding to the scattering by the point defects corresponding to the doping sites. Our findings thus not only provide a qualitative explanation for recent transport measurements, but are also the first direct identification of the nature and electronic properties of the nitrogen dopant sites in single-walled carbon nanotubes. A detailed understanding of the dopant structures is crucial for the design of nanoelectronic devices based on these materials.

METHODS

Nanotubes Growth and Sample Preparation. The nitrogen-doped single-walled carbon nanotubes (N-SWNTs) were synthesized using a gas-phase floating catalyst CVD method, where carbon monoxide (CO) acts as the carbon source, ammonia (NH_3) as the nitrogen source, and iron particles derived from physical nucleation of evaporated iron as the catalyst. The N-SWNTs were dry-deposited directly from the reactor using an *in situ* electric

field collector onto gold-coated glass substrates (Arrandee), which had been heat treated before collection to form Au(111) terraces. No solution processing, sonication, or centrifugation was thus applied, which ensured that the intrinsic properties of the material were preserved. The synthesis and characterization of thin films of the N-SWNTs were reported previously,[29] and the sample discussed here was collected concurrently with the samples denoted "300 ppm NH_3" in that work. For this batch of tubes, an average diameter of 1.1 $\pm$ 0.2 nm was determined by an analysis of optical absorption spectra.[29]

Scanning Tunneling Microscopy and Spectroscopy. STM/STS measurements were performed using an Omicron Nanotechnology low temperature (5K) STM operating under UHV conditions (less than 10^{-10} mbar). Local d*I*/d*V* spectra were recorded with LT-STM using a lock-in amplifier with a modulation at *ca*. 750 Hz and 20 mV. The samples were introduced into the UHV system and outgassed for 2 h at a temperature of 420 K to remove residual adsorbed molecules. All measurements were performed with electrochemically etched tungsten tips.

DFT Calculations. The SIESTA package[48] was used for the *ab initio* DFT calculations of the electronic structure of the nanotube. The description of the valence electrons was based on localized pseudoatomic orbitals with a double-ζ (DZ) basis.[49] Exchange-correlation effects were handled within the local density approximation (LDA) as proposed by Perdew and Zunger.[50] Core electrons were replaced by nonlocal norm-conserving pseudopotentials,[51] and real-space integration performed on a regular grid corresponding to a plane-wave cutoff around 300 Ry. The atomic structure of the self-supported doped nanotube was fully relaxed. For the simulation of the STM images, the standard Tersoff–Hamann's model[34,35] was implemented.[17] The simulations were performed on a periodically repeating system consisting of a (11,5) unit cell (268 atoms, cell length 20.13 Å along the tube axis) with a single substituted N atom; the influence of the gold substrate is neglected in this approach. A grid of 40 points in the reciprocal space was used for the calculation of the density of states (DOS).[52] No major atomic relaxation was observed after geometry optimization, in agreement with previous work.[17]

Conflict of Interest: The authors declare no competing financial interest.

Acknowledgment. Y.T. thanks H. Amara and F. Joucken for fruitful discussions. This study has been supported by the European STREP project BNC Tubes (Contract 30007654-OTP25763), by a grant from CNano IdF Samba project, by the SESAME project and by the ANR project CEDONA of the PNANO programme (ANR-07-NANO-00702). V.R. acknowledges support from the Institut Universitaire de France. *Ab initio* calculations were performed on resources from the plate-forme technologique en calcul intensif (PTCI) of the University of Namur, Belgium, for which the financial support of the F.R.S.-FNRS (Convention No. 2.4617.07. and 2.5020.11.) and of the FUNDP are acknowledged.

Supporting Information Available: STM image of a N-induced point defect with a triangular structure, simulated STM images of N-doped graphene at various tip-to-sample distances, and calculated densities of states for a (17,0) nanotube with a pyridinic configuration. This material is available free of charge *via* the Internet at http://pubs.acs.org.

REFERENCES AND NOTES

1. Iijima, S. Helical Microtubules of Graphitic Carbon. *Nature* **1991**, *354*, 56–58.
2. Loiseau, A.; Launois, P.; Petit, P.; Roche, S.; Salvetat, J. *Understanding Carbon Nanotubes*; Lecture Notes in Physics; Springer: New York, 2006; Vol. 677
3. Jorio, A.; Dresselhaus, G.; Dresselhaus, M. S. In *Carbon Nanotubes*; Jorio, A., Dresselhaus, G., Dresselhaus, M. S., Eds.; Topics in Applied Physics; Springer: New York, 2008; Vol. 111.
4. Ayala, P.; Arenal, R.; Loiseau, A.; Rubio, A.; Pichler, T. The Physical and Chemical Properties of Heteronanotubes. *Rev. Mod. Phys.* **2010**, *82*, 1843–1885.
5. Ayala, P.; Arenal, R.; Rümmeli, M.; Rubio, A.; Pichler, T. The Doping of Carbon Nanotubes with Nitrogen and Their Potential Applications. *Carbon* **2010**, *48*, 575–586.
6. Ghosh, K.; Kumar, M.; Maruyama, T.; Ando, Y. Tailoring the Field Emission Property of Nitrogen-Doped Carbon Nanotubes by Controlling the Graphitic/Pyridinic Substitution. *Carbon* **2010**, *48*, 191–200.
7. Krstic, V.; Rikken, G. L. J. A.; Bernier, P.; Roth, S.; Glerup, M. Nitrogen Doping of Metallic Single-Walled Carbon Nanotubes: n-Type Conduction and Dipole Scattering. *Europhys. Lett.* **2007**, *77*, 37001.
8. Peng, S.; Cho, K. *Ab Initio* Study of Doped Carbon Nanotube Sensors. *Nano Lett.* **2003**, *3*, 513–517.
9. Gong, K.; Du, F.; Xia, Z.; Durstock, M.; Dai, L. Nitrogen-Doped Carbon Nanotube Arrays with High Electrocatalytic Activity for Oxygen Reduction. *Science* **2009**, *323*, 760–764.
10. Glerup, M.; Steinmetz, J.; Samaille, D.; Stephan, O.; Enouz, S.; Loiseau, A.; Roth, S.; Bernier, P. Synthesis of N-doped SWNT Using the Arc-Discharge Procedure. *Chem. Phys. Lett.* **2004**, *387*, 193–197.
11. Villalpando-Paez, F.; Zamudio, A.; Elias, A.; Son, H.; Barros, E.; Chou, S.; Kim, Y.; Muramatsu, H.; Hayashi, T.; Kong, J.; *et al.* Synthesis and Characterization of Long Strands of Nitrogen-Doped Single-Walled Carbon Nanotubes. *Chem. Phys. Lett.* **2006**, *424*, 345–352.
12. Susi, T.; Nasibulin, A. G.; Ayala, P.; Tian, Y.; Zhu, Z.; Jiang, H.; Roquelet, C.; Garrot, D.; Lauret, J.-S.; Kauppinen, E. I. High Quality SWCNT Synthesis in the Presence of NH_3 Using a Vertical Flow Aerosol Reactor. *Phys. Status Solidi B* **2009**, *246*, 2507–2510.
13. Lin, H.; Lagoute, J.; Chacon, C.; Arenal, R.; Stephan, O.; Repain, V.; Girard, Y.; Enouz, S.; Bresson, L.; Rousset, S.; *et al.* Combined STM/STS, TEM/EELS Investigation of CN_x-SWNTs. *Phys. Status Solidi B* **2008**, *245*, 1986–1989.
14. Lin, H.; Arenal, R.; Enouz-Vedrenne, S.; Stephan, O.; Loiseau, A. Nitrogen Configuration in Individual CN_x-SWNTs Synthesized by Laser Vaporization Technique. *J. Phys. Chem. C* **2009**, *113*, 9509–9511.
15. Terrones, M.; Redlich, P.; Grobert, N.; Trasobares, S.; Hsu, W.-K.; Terrones, H.; Zhu, Y.-Q.; Hare, J. P.; Reeves, C. L.; Cheetham, A. K.; et al. Carbon Nitride Nanocomposites: Formation of Aligned C_xN_y Nanofibers. *Adv. Mater.* **1999**, *11*, 655–658.
16. Ibrahim, E.; Khavrus, V. O.; Leonhardt, A.; Hampel, S.; Oswald, S.; Rümmeli, M. H.; Bühner, B. Synthesis, Characterization, and Electrical Properties of Nitrogen-Doped Single-Walled Carbon Nanotubes with Different Nitrogen Content. *Diamond Relat. Mater.* **2010**, *19*, 1199–1206.
17. Zheng, B.; Hermet, P.; Henrard, L. Scanning Tunneling Microscopy Simulations of Nitrogen- and Boron-Doped Graphene and Single-Walled Carbon Nanotubes. *ACS Nano* **2010**, *4*, 4165–4173.
18. Ewels, C. P.; Glerup, M. Nitrogen Doping in Carbon Nanotubes. *J. Nanosci. Nanotechnol.* **2005**, *5*, 1345–1363.
19. Wildoer, J. W. G.; Venema, L. C.; Rinzler, A. G.; Smalley, R. E.; Dekker, C. Electronic Structure of Atomically Resolved Carbon Nanotubes. *Nature* **1998**, *391*, 59–62.
20. Odom, T. W.; Huang, J.-L.; Kim, P.; Lieber, C. M. Atomic Structure and Electronic Properties of Single-Walled Carbon Nanotubes. *Nature* **1998**, *391*, 62–64.
21. Czerw, R.; Terrones, M.; Charlier, J. C.; Blase, X.; Foley, B.; Kamalakaran, R.; Grobert, N.; Terrones, H.; Tekleab, D.; Ajayan, P. M.; et al. Identification of Electron Donor States in N-doped Carbon Nanotubes. *Nano Lett.* **2001**, *1*, 457–460.
22. Lin, H.; Lagoute, J.; Repain, V.; Chacon, C.; Girard, Y.; Lauret, J.-S.; Arenal, R.; Ducastelle, F.; Rousset, S.; Loiseau, A. Coupled Study by TEM/EELS and STM/STS of Electronic Properties of C- and CN_x-Nanotubes. *C. R. Phys.* **2011**, *12*, 909–920.
23. Zhao, L.; He, R.; Rim, K. T.; Schiros, T.; Kim, K. S.; Zhou, H.; Gutierrez, C.; Chockalingam, S. P.; Arguello, C. J.; Palova, L.; *et al.* Visualizing Individual Nitrogen Dopants in Monolayer Graphene. *Science* **2011**, *333*, 999–1003.

24. Deng, D.; Pan, X.; Yu, L.; Cui, Y.; Jiang, Y.; Qi, J.; Li, W.-X.; Fu, Q.; Ma, X.; Xue, Q.; et al. Toward N-Doped Graphene *via* Solvothermal Synthesis. *Chem. Mater.* **2011**, *23*, 1188–1193.
25. Joucken, F.; Tison, Y.; Lagoute, J.; Dumont, J.; Cabosart, D.; Zheng, B.; Repain, V.; Chacon, C.; Girard, Y.; Botello-Mèndez, A. R.; *et al*. Localized State and Charge Transfer in Nitrogen-Doped Graphene. *Phys. Rev. B: Condens. Matter Mater. Phys.* **2012**, *85*, 161408.
26. Lv, R.; Li, Q.; Botello-Mendez, A. R.; Hayashi, T.; Wang, B.; Berkdemir, A.; Hao, Q.; Elias, A. L.; Cruz-Silva, R.; Gutierrez, H. R. *et al*. Nitrogen-Doped Graphene: Beyond Single Substitution and Enhanced Molecular Sensing. *Sci. Rep.* **2012**, *2*, 10.1038/srep00586.
27. Lin, H.; Lagoute, J.; Repain, V.; Chacon, C.; Girard, Y.; Lauret, J.-S.; Ducastelle, F.; Loiseau, A.; Rousset, S. Many-Body Effects in Electronic Bandgaps of Carbon Nanotubes Measured by Scanning Tunnelling Spectroscopy. *Nat. Mater.* **2010**, *9*, 235–238.
28. Lin, H.; Lagoute, J.; Repain, V.; Chacon, C.; Girard, Y.; Ducastelle, F.; Amara, H.; Loiseau, A.; Hermet, P.; Henrard, L.; et al. Imaging the Symmetry Breaking of Molecular Orbitals in Single-Wall Carbon Nanotubes. *Phys. Rev. B: Condens. Matter Mater. Phys.* **2010**, *81*, 235412.
29. Susi, T.; Kaskela, A.; Zhu, Z.; Ayala, P.; Arenal, R.; Tian, Y.; Laiho, P.; Mali, J.; Nasibulin, A. G.; Jiang, H.; *et al*. Nitrogen-Doped Single-Walled Carbon Nanotube Thin Films Exhibiting Anomalous Sheet Resistances. *Chem. Mater.* **2011**, *23*, 2201–2208.
30. Wassmann, T.; Seitsonen, A. P.; Saitta, A. M.; Lazzeri, M.; Mauri, F. The thermodynamic stability and simulated STM images of graphene nanoribbons. *Phys. Status Solidi B* **2009**, *246*, 2586–2591.
31. Ouyang, M.; Huang, J.-L.; Cheung, C. L.; Lieber, C. M. Energy Gaps in "Metallic" Single-Walled Carbon Nanotubes. *Science* **2001**, *292*, 702–705.
32. Kataura, H.; Kumazawa, Y.; Maniwa, Y.; Umezu, I.; Suzuki, S.; Ohtsuka, Y.; Achiba, Y. Optical Properties of Single-Wall Carbon Nanotubes. *Synth. Met.* **1999**, *103*, 2555–2558.
33. Kondo, T.; Casolo, S.; Suzuki, T.; Shikano, T.; Sakurai, M.; Harada, Y.; Saito, M.; Oshima, M.; Trioni, M. I.; Tantardini, G. F.; et al. Atomic-Scale Characterization of Nitrogen-Doped Graphite: Effects of Dopant Nitrogen on the Local Electronic Structure of the Surrounding Carbon Atoms. *Phys. Rev. B: Condens. Matter Mater. Phys.* **2012**, *86*, 035436.
34. Tersoff, J.; Hamann, D. Theory and Application for the Scanning Tunneling Microscope. *Phys. Rev. Lett.* **1983**, *50*, 1998–2001.
35. Tersoff, J.; Hamann, D. R. Theory of the Scanning Tunneling Microscope. *Phys. Rev. B: Condens. Matter Mater. Phys.* **1985**, *31*, 805–813.
36. Lambin, P.; Amara, H.; Ducastelle, F.; Henrard, L. Long-Range Interactions between Substitutional Nitrogen Dopants in Graphene: Electronic Properties Calculations. *Phys. Rev. B: Condens. Matter Mater. Phys.* **2012**, *86*, 045448.
37. Barone, V.; Peralta, J. E.; Wert, M.; Heyd, J.; Scuseria, G. E. Density Functional Theory Study of Optical Transitions in Semiconducting Single-Walled Carbon Nanotubes. *Nano Lett.* **2005**, *5*, 1621–1624.
38. Tolvanen, A.; Buchs, G.; Ruffieux, P.; Groening, P.; Groening, O.; Krasheninnikov, A. V. Modifying the Electronic Structure of Semiconducting Single-Walled Carbon Nanotubes by Ar^+ Ion Irradiation. *Phys. Rev. B: Condens. Matter Mater. Phys.* **2009**, *79*, 125430.
39. Krasheninnikov, A. V. Predicted Scanning Tunneling Microscopy Images of Carbon Nanotubes with Atomic Vacancies. *Solid State Commun.* **2001**, *118*, 361–365.
40. Krasheninnikov, A. V.; Nordlund, K.; Sirviö, M.; Salonen, E.; Keinonen, J. Formation of Ion-Irradiation-Induced Atomic-Scale Defects on Walls of Carbon Nanotubes. *Phys. Rev. B: Condens. Matter Mater. Phys.* **2001**, *63*, 245405.
41. Clauss, W.; Bergeron, D. J.; Freitag, M.; Kane, C. L.; Mele, E. J.; Johnson, A. T. Electron Backscattering on Single-Wall Carbon Nanotubes Observed by Scanning Tunneling Microscopy. *Europhys. Lett.* **1999**, *47*, 601.
42. Kane, C. L.; Mele, E. J. Broken Symmetries in Scanning Tunneling Images of Carbon Nanotubes. *Phys. Rev. B: Condens. Matter Mater. Phys.* **1999**, *59*, R12759–R12762.
43. Buchs, G.; Ruffieux, P.; Groning, P.; Groning, O. Scanning Tunneling Microscopy Investigations of Hydrogen Plasma-Induced Electron Scattering Centers on Single-Walled Carbon Nanotubes. *Appl. Phys. Lett.* **2007**, *90*, 013104.
44. Furuhashi, M.; Komeda, T. Chiral Vector Determination of Carbon Nanotubes by Observation of Interference Patterns Near the End Cap. *Phys. Rev. Lett.* **2008**, *101*, 185503.
45. Krasheninnikov, A. V. Theoretical STM Images of Carbon Nanotubes with Atomic Vacancies: A Systematic Tight-Binding Study. *Phys. Low-Dim Struct.* **2000**, *11/12*, 1–24.
46. Latil, S.; Roche, S.; Mayou, D.; Charlier, J.-C. Mesoscopic Transport in Chemically Doped Carbon Nanotubes. *Phys. Rev. Lett.* **2004**, *92*, 256805.
47. Liu, Y.; Jin, Z.; Wang, J.; Cui, R.; Sun, H.; Peng, F.; Wei, L.; Wang, Z.; Liang, X.; Peng, L. Nitrogen-Doped Single-Walled Carbon Nanotubes Grown on Substrates: Evidence for Framework Doping and Their Enhanced Properties. *Adv. Funct. Mater.* **2011**, *21*, 986–992.
48. Sánchez-Portal, D.; Ordejón, P.; Artacho, E.; Soler, J. M. Density-Functional Method for Very Large Systems with LCAO Basis Sets. *Int. J. Quantum Chem.* **1997**, *65*, 453–461.
49. Artacho, E.; Sánchez-Portal, D.; Ordejón, P.; García, A.; Soler, J. M. Linear-Scaling *Ab-Initio* Calculations for Large and Complex Systems. *Phys. Status Solidi B* **1999**, *215*, 809–817.
50. Perdew, J. P.; Zunger, A. Self-Interaction Correction to Density-Functional Approximations for Many-Electron Systems. *Phys. Rev. B: Condens. Matter Mater. Phys.* **1981**, *23*, 5048–5079.
51. Troullier, N.; Martins, J. L. Efficient Pseudopotentials for Plane-Wave Calculations. *Phys. Rev. B: Condens. Matter Mater. Phys.* **1991**, *43*, 1993–2006.
52. Monkhorst, H. J.; Pack, J. D. Special Points for Brillouin-Zone Integrations. *Phys. Rev. B: Solid State* **1976**, *13*, 5188–5192.